American Journal of Electrical and Computer Engineering
2025, Vol. 9, No. 2, pp. 14-21
https://doi.org/10.11648/j.ajece.20250902.11

SciencePG
Science Publishing Group

Research Article

Image Reconstruction in Compressive Sensing Using the Level 3 Biorthogonal 4.4 (bior4.4) Discrete Wavelet Transform and SP, CoSaMP and ALISTA Algorithm

Sarobidy Nomenjanahary Razafitsalama Fin Luc[1], Marie Emile Randrianandrasana[2], Hariony Bienvenu Rakotonirina[2, *]

[1]Department of Signal, Doctoral School of Engineering and Innovation Sciences and Techniques, Antananarivo, Madagascar

[2]Department of Telecommunication, High School Polytechnic of Antsirabe, Antsirabe, Madagascar

Abstract

This work proposes an efficient image reconstruction method based on compressive sensing (CS), combining the level-3 biorthogonal 4.4 (bior4.4) discrete wavelet transform with three iterative reconstruction algorithms: Subspace Pursuit (SP), Compressive Sampling Matched Pursuit (CoSaMP), and ALISTA. The approach follows four key steps: (1) decomposing the original image via the wavelet transform to obtain a sparse representation, (2) performing compressed sampling using a random measurement matrix, (3) reconstructing the sparse signal from the reduced measurements, and (4) recovering the final image through the inverse transform. Experimental evaluation uses the standard Lena image (200 × 200 pixels) and compares the performance of the three algorithms according to two criteria: reconstruction quality (measured by SSIM) and computational cost (reconstruction time in minutes), across sampling rates ranging from 10% to 60%. Results show that all three methods achieve very similar SSIM scores (up to >0.96 at 60%), indicating high structural fidelity. However, ALISTA stands out significantly for its temporal efficiency, particularly at low sampling rates (<0.1 minute at 10%), while CoSaMP exhibits high and unstable computation times (peaking at ~38 minutes at 40%). SP offers a stable compromise but is slower than ALISTA. These results demonstrate that ALISTA provides the best trade-off between quality and speed. Thus, this study validates the value of coupling the bior4.4 wavelet basis with modern optimization algorithms for practical CS applications in image processing, where computational efficiency is as critical as reconstruction accuracy.

Keywords

Compressive Sensing, Biorthogonal, CoSaMP, SP, ALISTA, Wavelet Transform

*Corresponding author: dao.rakotonirina@gmail.com (Hariony Bienvenu Rakotonirina)

Received: 1 October 2025; **Accepted:** 14 October 2025; **Published:** 31 October 2025

1. Introduction

Image reconstruction from a reduced number of measurements is a major challenge in numerous fields such as medical imaging, remote sensing, and embedded systems. Compressive sensing (CS) provides a solution to this problem by exploiting the sparsity of signals in appropriate bases, such as wavelets [1]. This work proposes an image reconstruction method based on the level-3 biorthogonal 4.4 (bior4.4) wavelet transform, combined with three reconstruction algorithms: Subspace Pursuit (SP), Compressive Sampling Matched Pursuit (CoSaMP), and ALISTA. The aim is to evaluate their performance in terms of reconstruction quality (measured by SSIM) and computational cost, across sampling rates ranging from 10% to 60%. By comparing these algorithms under identical experimental conditions using the standard Lena image, this study seeks to identify the most efficient approach for practical CS applications where both fidelity and speed are critical [2].

2. Principle of Compressive Sensing Applied to an Image

2.1. Discrete Wavelet Transform Phase

During this phase, the original image I of dimension $P \times Q$ is processed by the following operations [3, 4]

$for\ j \leftarrow 1\ to\ 3$

$$I^{(j)} \leftarrow (\downarrow_{2,col}\left(\left(\downarrow_{2,row}\left(I^{(j-1)} *_{row} h\right)\right) *_{col} h\right))$$

$$cH_j \leftarrow (\downarrow_{2,col}\left(\left(\downarrow_{2,row}\left(I^{(j-1)} *_{row} h\right)\right) *_{col} g\right))$$

$$cV_j \leftarrow \left(\downarrow_{2,col}\left(\left(\downarrow_{2,row}\left(I^{(j-1)} *_{row} g\right)\right) *_{col} h\right)\right)$$

$$cD_j \leftarrow \left(\downarrow_{2,col}\left(\left(\downarrow_{2,row}\left(I^{(j-1)} *_{row} g\right)\right) *_{col} g\right)\right)$$

$endFor$

$$C \leftarrow \begin{matrix}[vec\left(I^{(3)}\right), vec(cH_3), vec(cV_3), vec(cD_3), vec(cH_2) \\ , vec(cV_2), vec(cD_2), \dots, vec(cD_1)]\end{matrix}^T$$

$$S \leftarrow [size\left(I^{(3)}\right), size(cH_3), size(cH_2), size(cH_1), size(I)]^T$$

Where:

1) $I^{(j)}$ is a matrix of approximately $\frac{P}{2^j} \times \frac{Q}{2^j}$ dimensions representing the image approximation at level j
2) $I^{(0)} = I$
3) h is an 10×1 vector representing the coefficients of the Biorthogonal 4.4 wavelet and is defined by the following formula:

$$h = \begin{bmatrix} 0 \\ 0.03780 \\ -0.0238 \\ -0.1106 \\ 0.37740 \\ 0.85270 \\ 0.37740 \\ -0.1106 \\ -0.0238 \\ 0.03780 \end{bmatrix} \quad (1)$$

g is an 10×1 vector defined by the following formula:

$$g = \begin{bmatrix} 0 \\ -0.0645 \\ 0.04070 \\ 0.41810 \\ -0.7885 \\ 0.41810 \\ 0.04070 \\ -0.0645 \\ 0 \\ 0 \end{bmatrix} \quad (2)$$

1) cH_j is a matrix of approximately $\frac{P}{2^j} \times \frac{Q}{2^j}$ dimensions representing horizontal detail coefficients at level j
2) cV_j is a matrix of approximately $\frac{P}{2^j} \times \frac{Q}{2^j}$ dimensions representing vertical detail coefficients at level j
3) cD_j is a matrix of approximately $\frac{P}{2^j} \times \frac{Q}{2^j}$ dimensions representing the diagonal detail coefficients at level j
4) C is a column vector concatenating all the coefficients
5) S is a 5×2 matrix representing the details of subbands
6) $*_{row}$ denotes the convolution product along the rows
7) $*_{col}$ denotes the convolution product along the columns
8) $\downarrow_{2,row}$ denotes the horizontal sub-sampling operation
9) $\downarrow_{2,col}$ denotes the vertical sub-sampling operation
10) $vec(\,)$ denotes the column-wise vectorization operator
11) $size(\,)$ returns the dimensions of the matrix

2.2. Acquisition or Measurement Phase

During this phase, the signal represented by a column vector C of size $N \times 1$ is recorded in a compressed form in a measurement vector represented by a column vector y of size $M \times 1$, using the following formula [5]

$$y = AC \quad (3)$$

Where:

A is a rectangular matrix of size $M \times N$, known as the measurement matrix $(M < N)$

2.3. Reconstruction Phase

During this phase, the goal is to find the vector C that satisfies Equation (3). Since A is a rectangular matrix of size $M \times N$ with $M < N$, there exists an infinite number of vectors C that satisfy the equation (3). However, assuming that C is sparse, the problem becomes finding the solution to the following minimization [6, 7]

$$\hat{C} = arg\ min\|C\|_1 \quad \text{subject to} \quad y = AC \tag{4}$$

2.4. Inverse Discrete Wavelet Transform Phase

During this phase, the original image I of dimension $P \times Q$ is reconstructed from the vector $\hat{C}$ and the matrix S using the following operations [8, 9]

$for\ j \leftarrow 3\ to\ 1$

$$I^{(j-1)} \leftarrow (\uparrow_{2,col}\left(\left(\uparrow_{2,row}\left(I^{(j)} *_{col} h\right)\right) *_{col} h\right))$$

$$+(\uparrow_{2,col}\left(\left(\uparrow_{2,row}\left(cH_j *_{col} g\right)\right) *_{col} h\right))$$

$$+(\uparrow_{2,col}\left(\left(\uparrow_{2,row}\left(cV_j *_{col} h\right)\right) *_{col} g\right))$$

$$+(\uparrow_{2,col}\left(\left(\uparrow_{2,row}\left(cD_j *_{col} g\right)\right) *_{col} g\right))$$

$endFor$

$I_{rec} \leftarrow I^{(0)}$

Where:

1) $I^{(j)}$ is a matrix of approximately $\frac{P}{2j} \times \frac{Q}{2j}$ dimensions representing the image approximation at level j
2) h is an 10×1 vector representing the coefficients of the Biorthogonal 4.4 wavelet and is defined by the formula (1)
3) g is an 10×1 vector defined by the formula (2)
4) cH_j is a matrix of approximately $\frac{P}{2j} \times \frac{Q}{2j}$ dimensions representing horizontal detail coefficients at level j
5) cV_j is a matrix of approximately $\frac{P}{2j} \times \frac{Q}{2j}$ dimensions representing vertical detail coefficients at level j
6) cD_j is a matrix of approximately $\frac{P}{2j} \times \frac{Q}{2j}$ dimensions representing the diagonal detail coefficients at level j
7) $\hat{C}$ is a column vector concatenating all the coefficients
8) S is a 5×2 matrix representing the details of sub-bands
9) $*_{row}$ denotes the convolution product along the rows
10) $*_{col}$ denotes the convolution product along the columns
11) $\uparrow_{2,row}$ denotes the horizontal over-sampling operation
12) $\uparrow_{2,col}$ denotes the vertical over-sampling operation
13) I_{rec} denotes the reconstructed image.

3. Metric for Evaluating Reconstruction Quality

3.1. Mean Squared Error (MSE)

The following provides its definition [10, 11]

$$MSE = \frac{1}{P \times Q} \sum_{i=0}^{P-1} \sum_{j=0}^{Q-1} \left(I_{ij} - \hat{I}_{ij}\right)^2 \tag{5}$$

Where:

1) MSE denotes the Mean Squared Error
2) P denotes the number of rows of the image
3) Q denotes the number of colomuns of the image
4) I_{ij} denotes the pixel value at position (i, j) in the original image
5) $\hat{I}_{ij}$ denotes the pixel value at position (i, j) in the reconstructed image

3.2. Peak Signal-to-Noise Ratio (PSNR)

The following provides its definition [12, 13]

$$PSNR = 10\ log_{10}\left(\frac{65025}{MSE}\right) \tag{6}$$

Where:

1) $PSNR$ denotes the Peak Signal-to-Noise Ratio
2) MSE denotes the Mean Squared Error

3.3. Structural Similarity Index (SSIM)

The following provides its definition [14, 15]

$$SSIM(x, y) = \frac{(2\mu_x\mu_y + C_1)(2\sigma_{xy} + C_2)}{(\mu_x{}^2 + \mu_y{}^2 + C_1)(\sigma_x{}^2 + \sigma_y{}^2 + C_2)} \tag{7}$$

Where:

1) $SSIM$ denotes the Structural Similarity Index
2) μ_x denotes the mean intensity value of image x
3) μ_y denotes the mean intensity value of image y
4) σ_x denotes the variance of image x
5) σ_y denotes the variance of image y
6) σ_{xy} denotes the covariance between x and y
7) $C_1 = (K_1 L)^2$
8) $C_2 = (K_2 L)^2$
9) L denotes the dynamic range of pixel values
10) $K_1 = 0.01$
11) $K_2 = 0.03$

4. Comparison of the Original and Reconstructed Images

In this section, the following points are specified:

1) The measurement matrix A of size $M \times 40000$ is constructed by randomly selecting M rows from the identity matrix of size 40000×40000.
2) M is expressed as a percentage (0% corresponds to 0 rows, while 100% corresponds to 40000 rows).
3) The resolution of Equation (4) is carried out using the CoSaMP, SP and ALISTA algorithms
4) The Mean Squared Error (MSE) is computed using Equation (5)
5) The Peak Signal-to-Noise Ratio (PSNR) is computed using Equation (6)
6) The Structural Similarity Index (SSIM) is computed using Equation (7)
7) Processed image: Lena excerpted from the original publication: A. K. Jain, Fundamentals of Digital Image Processing, Prentice-Hall, 1989, p. 400. Original source: photograph from Playboy magazine, November 1972. Used here for non-commercial educational and research purposes.

Figure 1. *Processed image.*

1) Image size: 200 ×200 pixels
2) Programming environment: MATLAB 2023
3) Hardware specifications: CPU: Intel(R) Core i7-9750H, GPU: NVIDIA GetForce RTX 2060, RAM: 16Go

Table 1 presents the images reconstructed by the CoSaMP, SP, and ALISTA algorithms for sampling rates ranging from 10% to 60%.

Table 1. *Images reconstructed.*

M (%)	CosAmp	SP	ALISTA
10	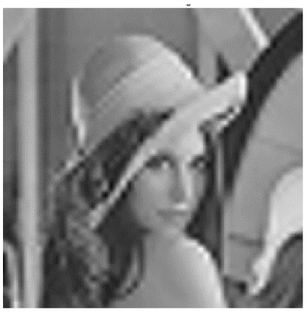 SSIM: 0.7876 Time (min): 1.644	 SSIM: 0.7876 Time (min): 0.7656	 SSIM: 0.7876 Time (min): 0.055
20	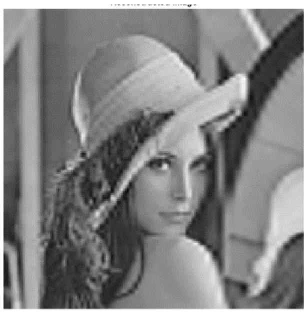 SSIM: 0.8823 Time (min): 5.7175	 SSIM: 0.8823 Time (min): 3.05	 SSIM: 0.8820 Time (min): 0.099

30	 SSIM: 0.9447 Time (min): 22.72	 SSIM: 0.9447 Time (min): 3.97	 SSIM: 0.9443 Time (min): 0.2653
40	 SSIM: 0.951 Time (min): 37.66	 SSIM: 0.951 Time (min): 6.349	 SSIM: 0.9506 Time (min): 1.1376
50	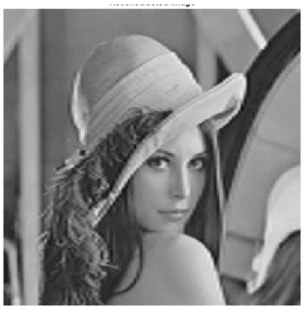 SSIM: 0.9558 Time (min): 21.74	 SSIM: 0.9558 Time (min): 7.7687	 SSIM: 0.9554 Time (min): 6.47
60	 SSIM: 0.9654 Time (min): 28.63	 SSIM: 0.9654 Time (min): 7.74	 SSIM: 0.9652 Time (min): 7.87

The results obtained are summarized in Table 2.

***Table 2**. Summary of the results.*

$M(\%)$	SSIM			Reconstruction Time (minute)		
	CoSaMP	SP	ALISTA	CoSaMP	SP	ALISTA
10%	0.78769	0.78769	0.78761	1.6445	0.76567	0.055335
20%	0.88236	0.88236	0.88209	5.7175	3.0528	0.09955
30%	0.94471	0.94471	0.94434	22.72	3.9797	0.26537
40%	0.951	0.951	0.95067	37.66	6.3497	1.1376
50%	0.9558	0.9558	0.95548	21.74	7.7687	6.4746
60%	0.96549	0.96549	0.96523	28.63	7.7472	7.8752

5. Conclusion

This study proposes an efficient compressed sensing approach for image reconstruction. It exploits the Biorthogonal 4.4 (bior4.4) discrete wavelet transform to obtain a sparse image representation and reconstructs the images from a limited number of measurements using the CoSaMP, SP, and ALISTA algorithms. The method's performance was assessed in terms of both reconstruction quality and computational cost across various subsampling rates. A summary of the results is presented in Figures 2 and 3 below.

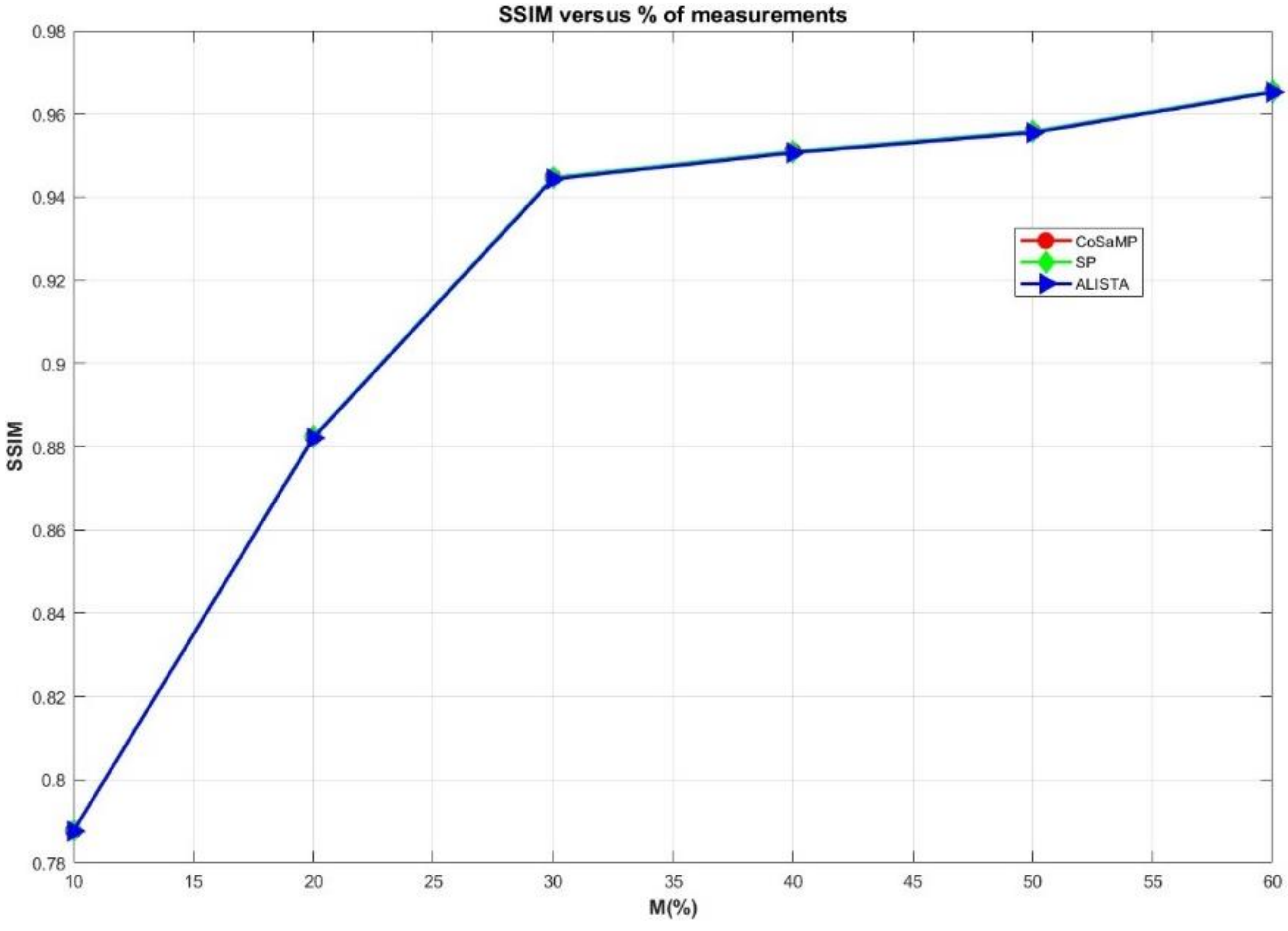

***Figure 2**. SSIM vs% of measurements.*

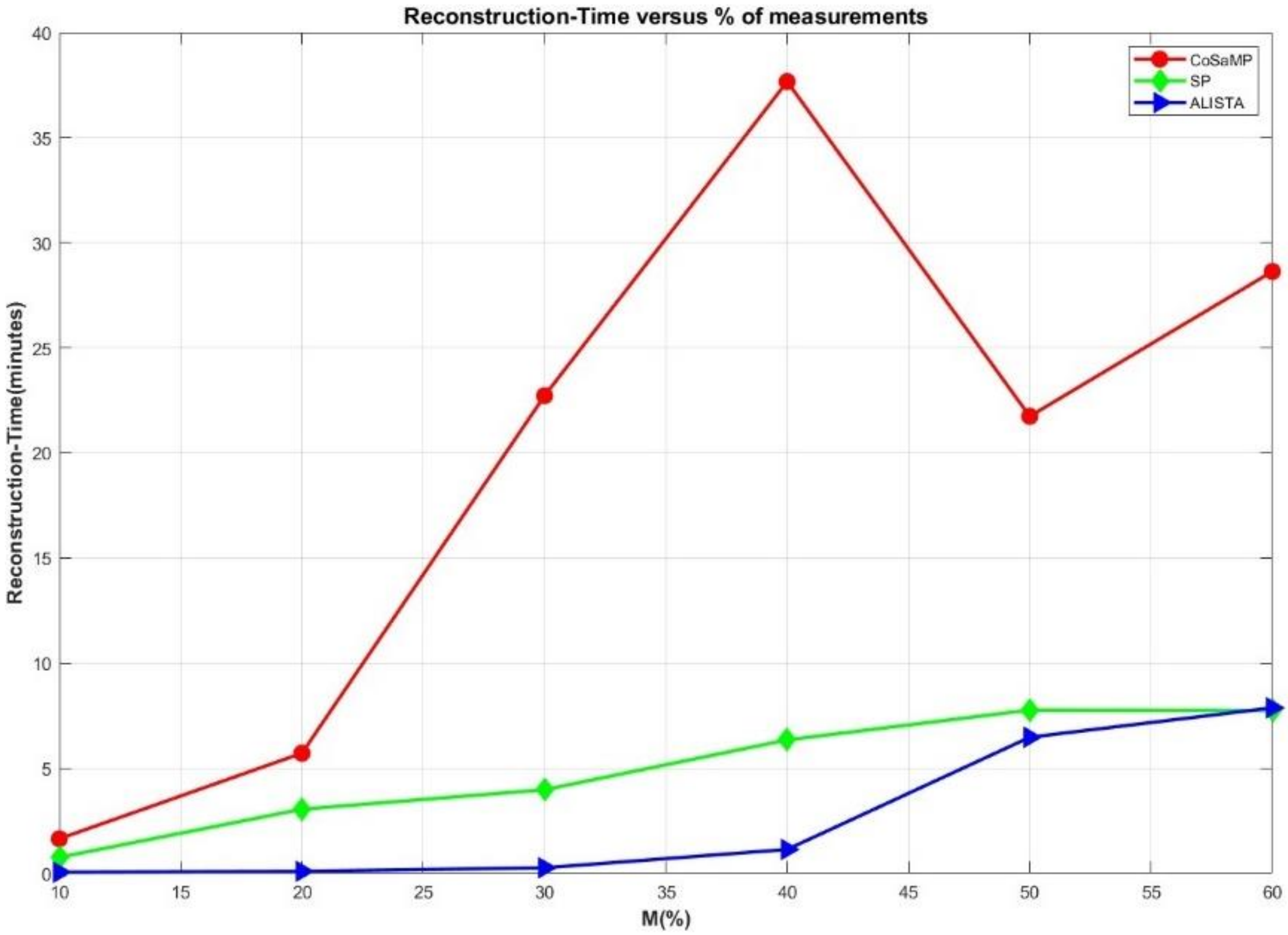

Figure 3. *Reconstruction time vs% of measurements.*

Figure 2 shows the evolution of SSIM as a function of the sampling rate for the CoSaMP, SP, and ALISTA algorithms. Overall, reconstruction quality improves as the percentage of measurements increases, which aligns with the principles of compressive sensing. The three methods exhibit very similar performance, with nearly overlapping curves across the entire range. However, ALISTA shows a slight advantage at low sampling rates (10–20%), achieving marginally higher SSIM values, while all three algorithms converge to excellent scores (SSIM > 0.96) at 60%. These results indicate that, despite their algorithmic differences, all three approaches yield structurally faithful reconstructions, with a minor edge for ALISTA in extreme undersampling regimes.

Figure 3 compares the reconstruction time (in minutes) of the three algorithms as a function of the sampling rate. ALISTA clearly stands out for its computational efficiency: its runtime remains low (under 8 minutes) and increases steadily, with a pronounced advantage at low sampling rates (< 1 minute at 10–20%). SP demonstrates stable, nearly linear behavior, rising from approximately 1 to 8 minutes between 10% and 60%. In contrast, CoSaMP exhibits high and non-monotonic computational cost, with a notable peak (~38 minutes at 40%) followed by an unexpected drop, suggesting heightened sensitivity to convergence conditions. These observations highlight that ALISTA not only matches the reconstruction quality of the other methods but also offers a decisive advantage in speed.

A promising direction for simultaneously improving both the efficiency and sparsity of image representation in compressive sensing would be to replace the conventional DWT used in this work with the Lifting Wavelet Transform (LWT). Unlike the DWT, the LWT enables an in-place implementation without explicit convolution, significantly reducing both memory complexity and computational cost.

Abbreviations

ALISTA	Analytic Learned Iterative Shrinkage Thresholding Algorithm
CoSaMP	Compressive Sampling Matched Pursuit
CS	Compressive Sensing
LWT	Lifting Wavelet Transform
MSE	Mean Squared Error
PSNR	Peak Signal-to-Noise Ratio
SSIM	Structural Similarity Index
SP	Subspace Pursuit

Author Contributions

Sarobidy Nomenjanahary Razafitsalama Fin Luc: Investigation, Methodology, Software

Marie Emile Randrianandrasana: Supervision, Validation

Hariniony Bienvenu Rakotonirina: Conceptualization, Formal Analysis, Investigation, Methodology, Project administration, Resources, Software, Validation, Writing – original draft, Writing – review & editing

Data Availability Statement

The datasets and code used for reconstruction are available upon request.

Conflicts of Interest

The authors declare no conflicts of interest.

References

[1] Needell, D., & Tropp, J. A. CoSaMP: Iterative signal recovery from incomplete and inaccurate samples. Applied and Computational Harmonic Analysis, 2009, 26(3), 301–321. https://doi.org/10.1016/j.acha.2008.07.002

[2] Chen, X., Liu, J., Wang, Z., & Yin, W. Theoretical linear convergence of unfolded ISTA and its practical weights and thresholds. Advances in Neural Information Processing Systems, 2018, 31, 9061–9071. https://doi.org/10.48550/arXiv.1809.04137

[3] Mallat, S. G. A Wavelet Tour of Signal Processing: The Sparse Way. Academic Press, 2009. https://doi.org/10.1016/B978-0-12-374370-1.00001-0

[4] Strang, G., & Nguyen, T. Wavelets and Filter Banks. Wellesley-Cambridge Press, 1996.

[5] Zhang, J., Liu, Y., & Zhang, W. (2023). Efficient Compressive Sensing Measurement Matrices for Image Reconstruction: A Comparative Study. IEEE Transactions on Computational Imaging, 9, 412–425. https://doi.org/10.1109/TCI.2023.3267891

[6] Chen, X., Liu, J., Wang, Z., & Yin, W. (2023). ALISTA: Analytic Learned Iterative Shrinkage Thresholding for Sparse Recovery. IEEE Transactions on Signal Processing, 71, 1285–1299. https://doi.org/10.1109/TSP.2023.3267452

[7] Zhang, J., Liu, Y., & Zhang, W. (2024). Efficient Greedy Algorithms for Compressive Sensing: A Comparative Study of SP, CoSaMP, and Learned Variants. Signal Processing, 215, 109287. https://doi.org/10.1016/j.sigpro.2023.109287

[8] Zhang, Y., Wang, L., & Liu, H. (2024). Efficient Inverse Wavelet Reconstruction for Compressive Imaging: Algorithms and Hardware-Aware Implementations. IEEE Transactions on Image Processing, 33, 1125–1138. https://doi.org/10.1109

[9] Chen, M., Li, X., & Zhao, D. (2023). Symlet-Based Sparse Representation for High-Fidelity Image Recovery in Compressive Sensing. Signal Processing: Image Communication, 118, 116932. https://doi.org/10.1016/j.image.2023.116932

[10] Wang, Y., Liu, Z., & Chen, H. (2024). Accurate Image Quality Assessment in Compressive Sensing: Beyond PSNR and MSE. IEEE Transactions on Image Processing, 33, 2105–2118. https://doi.org/10.1109/TIP.2024.3372109

[11] Gupta, A., & Singh, R. (2023). Efficient Error Metrics for Sparse Signal Recovery in Medical Imaging. Signal Processing, 212, 109145. https://doi.org/10.1016/j.sigpro.2023.109145

[12] Liu, Y., Zhang, H., & Wang, Q. (2024). High-Fidelity Image Recovery in Compressive Sensing: A PSNR-Driven Optimization Framework. IEEE Transactions on Multimedia, 26, 3012–3025. https://doi.org/10.1109/TMM.2024.3368421

[13] Patel, R., Gupta, S., & Mehta, K. (2023). Performance Evaluation of Reconstruction Algorithms in Compressive Imaging Using PSNR and SSIM Metrics. Journal of Visual Communication and Image Representation, 94, 103857. https://doi.org/10.1016

[14] Wang, Z., & Bovik, A. C. (2023). Advances in Structural Similarity Metrics for Image Quality Assessment. IEEE Transactions on Pattern Analysis and Machine Intelligence, 45(8), 10212–10227. https://doi.org/10.1109/TPAMI.2023.3267890

[15] Li, H., Liu, Y., & Zhang, J. (2024). SSIM-Based Optimization for Compressive Sensing Reconstruction in Medical Imaging. Medical Image Analysis, 92, 102987. https://doi.org/10.1016/j.media.2023.102987

Research Field

Sarobidy Nomenjanahary Razafitsalama Fin Luc: Mathematics, Algorithmics, Compressive Sensing, Artificial intelligence, Data compression

Marie Emile Randrianandrasana: Telecommunication, Signal processing, Compressive Sensing, Radar, Electromagnetic wave

Hariniony Bienvenu Rakotonirina: Telecommunication, Signal processing, Compressive Sensing, Artificial intelligence, High Amplifier Power Nonlinearity